Spatial Soliton Pixels in Semiconductor Devices

M. Brambilla,[1] L. A. Lugiato,[2] F. Prati,[3] L. Spinelli,[2] and W. J. Firth[4]
[1]*INFM, Dipartimento Interateneo di Fisica del Politecnico di Bari, via E.Orabona 4, 7016 Bari, Italy*
[2]*INFM, Dipartimento di Fisica dell' Università di Milano, via Celoria 16, 20133 Milano, Italy*
[3]*INFM, Università di Milano, II Facoltà di Scienze, via Lucini 3, 22100 Como, Italy*
[4]*Department of Physics and Applied Physics, University of Strathclyde, Glasgow G4 0NG, Scotland*
(Received 22 April 1997)

Semiconductor devices are the most appealing systems for information encoding using two-dimensional spatial solitons, recently reported both theoretically and experimentally in model systems. We show that stable solitons can be realized and controlled, both in passive microresonators with excitonic nonlinearity and in below-threshold vertical-cavity lasers. The solitons are robust enough to withstand significant carrier diffusion and self-defocusing, which is very encouraging for device applications. [S0031-9007(97)03963-X]

PACS numbers: 42.65.Tg, 42.65.Sf, 42.79.Ta

The extensive work in the field of transverse spatial pattern formation in nonlinear optical systems [1] was motivated, in part, by the hope of realizing applications to information technology. The main difficulty is the fact that the various parts of an optical pattern are strongly correlated, so that any local modification introduced to encode information either affects other parts or is spontaneously eliminated. This problem, however, can be circumvented by generating spatial solitons (SS) in a system constituted by a nonlinear material contained in a planar optical resonator driven by a stationary, coherent plane wave field [2–5], because the SS can be addressed individually and independently from one another.

Let us focus on the case when SS arise in the neighborhood of a modulational instability [3–5]. The idea is of considering the transverse planes, orthogonal to the propagation direction of the beam, as a blackboard on which light dots can be written and erased in any desired location. This is obtained by shining localized address pulses which locally create a bleached area, hence the name of "optical bullet holes" (OBH) [4] used for this kind of SS. This area exerts a guiding action on the optical field which counterbalances the spreading action of diffraction, making the soliton structure self-sustaining. The basic property which characterizes OBH with respect to the SS studied earlier is that, once they have been created, they persist until they are wiped out by another laser pulse; the presence of an optical cavity ensures this behavior.

Such SS arise even in the absence of any refractive effects; the analysis of Refs. [4,5] was based on a model in which the medium is a saturable absorber in exact resonance with radiation. Stable OBH have been found also in a Kerr medium model in a small parametric domain [6].

There is the possibility of fixing the position of SS by introducing a spatial modulation in the driving field [4] and of erasing them by introducing an appropriate phase shift in the address pulse [5]; in this way one may realize an optical memory array of soliton pixels, with $2^{N\times N}$ coexisting states for an array of $N \times N$ solitons. Recent experiments in liquid crystal light valves [7] and in organic saturable absorbers [8] confirmed the possibility of writing and erasing SS by laser pulses; the system in [8] corresponds closely to the model analyzed in [4,5].

A major breakthrough for SS application would be to demonstrate SS in semiconductor devices. In this paper we undertake a theoretical and numerical analysis of this problem, introducing suitable models for driven semiconductor (s.c.) microcavities to bridge the field of SS formation to the class of broad area s.c. optics. In our approach we introduce the two basic physical mechanisms which govern a s.c. material, namely, the carrier density dynamics coupled to that of the field via a proper modelization of the nonlinear interaction, and the carrier diffusion which is critically relevant for transverse effects. This increases substantially the numerical complexity of the models in comparison with those analyzed in [3–6] and in general with any sort of two-level model, because the transverse Laplacian appears in all equations. Diffusion represents a problem for the stability of SS, because it tends to quench them favoring the homogeneous state. Solitons arise from a balance between the guiding action of nonlinearity and the spreading action of diffraction, and one must see whether diffusion destroys this balance or not.

We consider a broad area s.c. heterostructure in a Fabry-Perot microresonator scheme in two basic configurations: (A) a passive (i.e., without injected current) multiple quantum well (MQW) structure perpendicular to the direction of propagation of the radiation, and (B) a vertical-cavity surface-emitting laser kept above transparency (hence with population inversion) but some 5%–10% below threshold. The active case (B) is considered in addition to the passive case (A) because passive s.c. devices can be typically operated only on the self-defocusing side of the resonance [9], and self-defocusing represents an additional problem for the stability of OBH. Introducing population inversion self-defocusing is converted into self-focusing, hence this problem is not met in case (B).

 0031-9007/97/79(11)/2042(4)$10.00

The paraxial model for both devices can be compactly cast as follows:

$$E_\tau = -[(1 + \eta + i\theta) + 2C\Theta D - i\nabla_\perp^2]E + E_I\,, \tag{1a}$$

$$D_\tau = -\gamma[(1 + |E|^2)D - 1 - \beta(1 - \sigma D)^2/\sigma - d\nabla_\perp^2 D]\,, \tag{1b}$$

where the subscript τ indicates differentiation with respect to τ, E and E_I are normalized slowly varying amplitudes associated with intracavity field and external driving field (homogeneous in the transverse plane), respectively; $D = (1 - N/N_0)/\sigma$, where N is the carrier density and N_0 is its transparency value. Time τ is scaled to the cavity decay rate κ and γ is the nonradiative carrier recombination rate normalized to κ. The Laplacian $\nabla_\perp^2 = \partial^2/\partial x^2 + \partial^2/\partial y^2$ describes diffractive and diffusive effects; the coordinates x, y are scaled to the diffraction length in the cavity $[\lambda\mathcal{L}/4\pi(1 - R)]^{1/2}$, where λ is the wavelength, $\mathcal{L}$ the cavity length, and R is the reflectivity coefficient of the mirrors; d is the squared ratio of the diffusion length to the diffraction length. The cavity mistuning from the input field frequency ω_0 is measured by θ [5]. Linear absorption (from Bragg reflectors, buffer layers, etc.) is accounted for by η; the term $(1 - \sigma D)^2 \propto N^2$ describes radiative recombination. In the *passive configuration* the nonlinearity is modeled via an excitonic resonance at ω_e described by a Lorentzian shape [10] with half-width γ_e, so $\Theta = (1 - i\Delta)/(1 + \Delta^2)$ where $\Delta = (\omega_e - \omega_0)/\gamma_e$. The bistability parameter C is defined as $C = \alpha_{\text{abs}} L\zeta/2(1 - R)$, where α_{abs} is the absorption coefficient per unit length on resonance, L is the length of the nonlinear medium, ζ is the confinement factor [10]; σ is equal to unity. In the *active configuration* a current J is supplied, larger than the transparency value J_0, thus making the medium inverted ($N > N_0$); $C \propto (J - J_0)$ is the pump parameter [11]; σ and Θ are defined, respectively, as $\sigma = 1 - J/J_0$ and $\Theta = i\alpha - 1$, where α is the linewidth enhancement factor of s.c. lasers [11].

The curve of the homogeneous (i.e., plane wave) steady state is derived from (1) by dropping all derivatives. An example of stationary curves for $|E|$ vs $|E_I|$ is given in Fig. 1 for both the passive and active cases. The linear stability analysis for the homogeneous stationary solutions was carried out analytically by evaluating the response of the system to perturbations of the form $\exp[i(K_x x + K_y y)]$. The instability domains in the plane $(|E|, K)$, where $K = (K_x^2 + K_y^2)^{1/2}$ and $|E|$ is the stationary value, are shown in Fig. 2 for different values of the parameter d. In Fig. 1 the unstable portions of the stationary curves are indicated by broken lines; those with positive slope correspond to modulational instabilities which form stationary patterns.

The scenario of emerging patterns has then been studied by extensive simulations using a split-step code with periodic boundary conditions. The numerical integration,

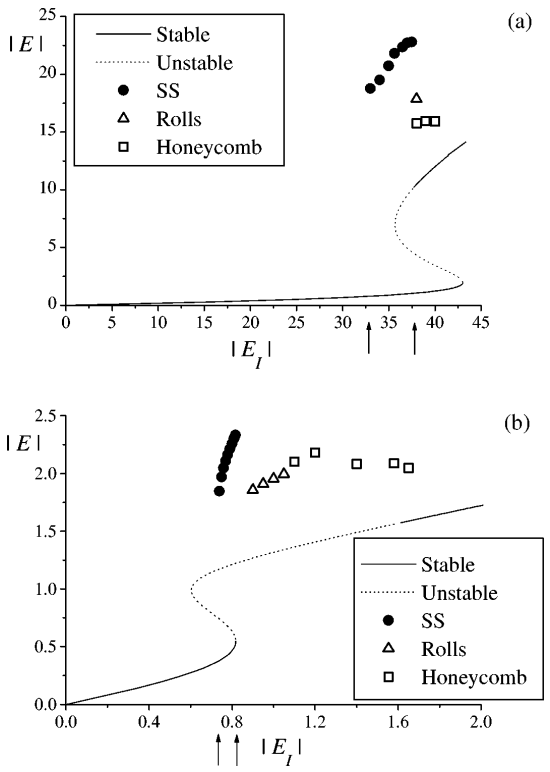

FIG. 1. Homogeneous steady-state curves with unstable domains and various patterns found by numerical simulations. (a) Passive case for $C = 40$, $\Delta = 1$ (self-defocusing), $\theta = -2$, $\eta = 0.25$, $\beta = 1.6$, $d = 0.2$. (b) Active case for $C = 0.45$ (threshold value $C = 0.5$), $\alpha = 5$, $\theta = -2$, $\eta = 0$, $\beta = 0$, $d = 0.052$.

a demanding task, is worsened by a stiffness stemming from the time rate γ in Eq. (1b) which is on the order of 10^{-2}–10^{-3}. It is thus critical to check the results from the integrations in time of the full model (1) using the radial integration technique formulated in [4]. It allows one to calculate the stationary SS directly, bypassing dynamical transients, so one gains a high spatial resolution and a reduced numerical load.

In our model the application of that approach is not straightforward. A first difficulty is the presence of one more equation (1b) with diffusion; a slightly different method is then adopted in which the radial integration is performed outwards (and not inwards as in [4]) from the origin $r = 0$ (at the SS peak), and we look for those initial values $E(r = 0) = E_0$, $D(r = 0) = D_0$, for which the solution integrated up to a fixed large value r_1 is as close as possible to the homogeneous solution. Looking for stationary, azimuthally symmetric solutions, the model is reduced to a set of ordinary differential equations

$$E_{rr} = iE_I + [\theta - i(1 + \eta)]E - 2Ci\Theta ED - E_r/r\,, \tag{2a}$$

$$D_{rr} = [(1 + |E|^2)D - 1 - \beta(1 - \sigma D)^2/\sigma]/d - D_r/r\,. \tag{2b}$$

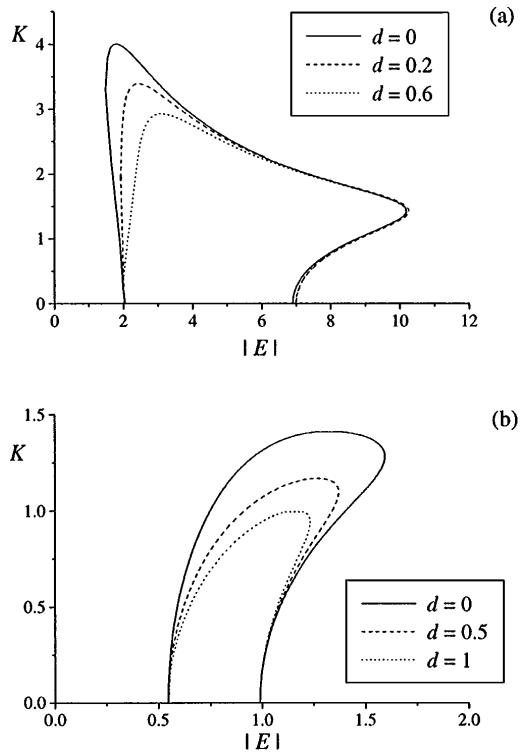

FIG. 2. The unstable region in the plane $(|E|, K)$ lies inside the curves, plotted for different values of d. (a) Passive case. (b) Active case. The other parameters are as in Fig. 1.

The integration of Eqs. (2) gives then a solution $(E(r; E_0, D_0), D(r; E_0, D_0))$ for each initial condition (E_0, D_0). Assuming that (E_h, D_h) is the homogeneous solution, a function

$$f(E_0, D_0) = \frac{1}{M} \sum_{m=0}^{M} [|E(r_1 - m\Delta r; E_0, D_0) - E_h|^2 + |D(r_1 - m\Delta r; E_0, D_0) - D_h|^2] \tag{3}$$

is defined which measures the distance between the calculated solution and the homogeneous one, where Δr is the integration step. The solutions we look for are the zeros of function f when $r_1 \to \infty$. The problem amounts to finding the minima of f in the 3D space of the parameters E_0 (complex) and D_0 (real).

A structural discrepancy from the saturable absorber scheme is the appearance of a further spatial scale factor, other than diffraction, due to the diffusion process. Experimental estimations of diffusion and diffraction lengths lead to values for d between 0.01 and 0.5, in both active and passive GaAs/GaAlAs structures. A stiffness appears via the smallness of d in the denominator of (2b) which renders the integration of Eqs. (2) sensitive to the choice of the initial condition (E_0, D_0): if it is not taken very close to the exact one, we are led to a rapid divergence as we move away from $r = 0$. This problem can be circumvented by applying a perturbative method. After expressing D in a power series of d, i.e., $D = D_0 + dD_1 + O(d^2)$, the expansion is inserted into Eqs. (1) which yields, up to terms of order d,

$$D_0 = [1 + (1 + |E|^2 - \sqrt{\mathcal{A}})/(2\beta)]/\sigma, \tag{4a}$$

$$D_1 = 2\{4(\beta + \sigma)[\mathrm{Re}(E^* E_r)]^2/(\sigma\mathcal{A}) - D_0[E_I \,\mathrm{Im}(E) + (\theta + 2CD_0 \,\mathrm{Im}(\Theta))|E|^2 + |E_r|^2]\}/\mathcal{A}, \tag{4b}$$

where $\mathcal{A} = (1 + |E|^2)^2 + 4\beta(1 + |E|^2 - \sigma)$ and we assumed E_I real. Hence Eqs. (2) reduce to only Eq. (2a) with $D = D_0 + dD_1$, the limit $d \to 0$ being now regular. Figure 3 shows the level of agreement obtained in the comparison between the results of the numerical integration in time and those of the radial integration; for all cases of interest we achieved an accuracy within 0.1%.

We explored selected but significant regions of the parameter space in order to identify the characteristic and general features of the results. In the passive case, the choice of parametric domains was suggested by the experimental results reported by CNET (see, e.g., [9]).

In Fig. 1 we indicate branches of different patterns that are found by numerical integration; we plot a value which corresponds to the maximum of $|E|$ in each pattern. As in the case of saturable absorber [4,5], a necessary condition to observe stable SS is the coexistence of a pattern branch with a portion of stable homogeneous steady-state branch; such a region is shown by arrows in Fig. 1. The kind of patterns (SS, rolls, honeycomb hexagons) as well as the location of the SS branch with respect to the homogeneous steady-state curve is qualitatively the same in the passive and in the active cases, and in the saturable absorber model, indicating a general scenario for the appearance of SS.

The most prominent fact that emerges from our calculations is that SS are robust with respect to carrier diffusion. When d is increased, the SS become lower and wider, and beyond a certain value $d_{\max}$ they do not exist any more. However, in self-focusing case (passive for $\Delta < 0$, active

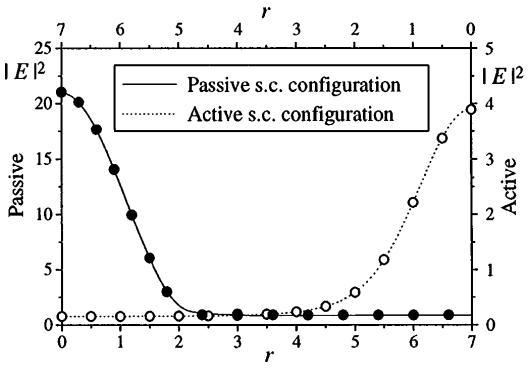

FIG. 3. Radial profile of the spatial soliton for both the passive (left) and the active (right) s.c. devices. The parameters used are $\eta = 0.25$, $\beta = 0$, $\theta = -3$, $C = 30$, $\Delta = 0$, $d = 0.2$, $|E_I| = 31$, and $\eta = 0$, $\beta = 0$, $\theta = -2$, $C = 0.45$, $\alpha = 5$, $d = 0.052$, $|E_I| = 0.75$, respectively, for the two cases. Results obtained by numerical simulations (symbols ● and ○) are compared to the radial integration results (solid and dotted lines).

for $\alpha > 0$) diffusion is not a problem as $d_{\max}$ is larger than the values one meets in practice.

Another interesting result is that, in the passive case, robust SS persist even in the presence of some defocusing [$\Delta > 0$; see Fig. 1(a)]. This means that the guiding action of saturation is strong enough to counterbalance the spreading effects arising from self-defocusing and diffusion. Of course, the amount of self-defocusing must be limited, e.g., for $20 < C < 40$, Δ must not exceed the value 1.6. The value of $d_{\max}$ is still not a problem when $\Delta = 1$: e.g., in the case of Fig. 1(a) $d_{\max} \approx 0.55$ for $|E_I| = 33$. Furthermore, the robustness of a SS to carrier diffusion increases with its height (i.e., with $|E_I|$).

For both active and passive systems, an increase of C produces an increase of the extension of the interval of input field $|E_I|$ where one meets stable SS.

When the modulus of the detuning parameter Δ (passive case) or α (active case) is of order unity, SS are found for negative values of the cavity mistuning θ; this feature arises from the interplay of cavity detuning and diffraction, described in [4].

The value of the rate γ in Eq. (1b) is basically irrelevant for the stationary patterns that emerge.

For the other parameters, we discuss the active and the passive cases separately.

(i) Passive systems.—We found stable SS when $|\Delta|$ is on the order of, or smaller than, unity; i.e., one must operate in a neighborhood of the excitonic resonance. In the self-focusing case $\Delta < 0$, for $30 < C < 40$, if $|\Delta|$ is significantly larger than unity one has still pattern formation, but isolated SS are not met; i.e., the creation of a SS also generates several other SS around it. As for the parameter β which governs radiative recombination, we considered the two values $\beta = 0$ and $\beta = 1.6$, and the picture is qualitatively the same; for $\beta = 1.6$ SS can resist to a stronger diffusion, especially in the self-defocusing case.

(ii) Active systems.—Stable solitons were found only when the linewidth enhancement factor α is positive, as it is usually; for $\alpha < 0$ we met spatial patterns but not solitons. For $\alpha > 0$, a reduction of α leads to the disappearance of SS, but this effect can be counteracted by increasing $|\theta|$.

In the paraxial approximation used in our model the width of SS scales as the diffraction length in the cavity. In the case of standard microresonators, the transmissivity coefficient $(1 - R)$ is small, so that a reduction in R would be beneficial to decrease the size of SS.

We analyzed in details the process of writing and erasing OBH; the picture remains basically that described in the saturable absorber case [5]. We found, in addition, that a SS can be erased even when the pulse is not aimed exactly; i.e., the system can self-accommodate some error.

The pulse duration for writing and erasing is on the order of the nonradiative recombination rate. To perform this operation, in the passive case our calculations indicate a pulse power of ≈ 0.5 mW which corresponds to a switching energy of ≈ 1.5 pJ; the intensity of the holding beam is on the order of 7 kW/cm^2. In the active case, in which the parameter C is quite lower, the switching power is ≈ 0.2 mW (which corresponds to 0.5 pJ), and the holding intensity is ≈ 0.7 kW/cm^2. No optimization of these figures was attempted.

The results of our theoretical and numerical investigations lead one to conclude that the realization of an array of spatial solitons using s.c. materials is feasible despite diffusion and, sometimes, self-defocusing. The parametric domains, where SS exist, are of sizable extent and accessible to experimental realizations. Both the active and the passive cases present promising perspectives; the first offers the advantages of presence of gain, which ensures cascadability, and of smaller holding and switching powers. The second is less noisy and exhibits more extended domains of holding beam intensity, where SS exist.

We thank R. Kuszelewicz for stimulating discussions. This research was carried out in the framework of the ESPRIT LTR Project PASS.

[1] L. A. Lugiato, Chaos Solitons Fractals **4**, 1251 (1994), and references therein.
[2] N. N. Rosanov, in *Progress in Optics*, edited by E. Wolf (North-Holland, Amsterdam, 1996), Vol. XXXV, pp. 1–57.
[3] M. Tlidi, P. Mandel, and R. Lefever, Phys. Rev. Lett. **73**, 640 (1994).
[4] W. J. Firth and A. J. Scroggie, Phys. Rev. Lett. **76**, 1623 (1996).
[5] M. Brambilla, L. A. Lugiato, and M. Stefani, Europhys. Lett. **34**, 109 (1996).
[6] W. J. Firth and A. Lord, J. Mod. Opt. **43**, 1071 (1996).
[7] B. Thüring, M. Kreuzer, A. Schreiber, and T. Tschudi, in *EQEC '96, Proceedings of the 1996 European Quantum Electronics Conference, Hamburg, 1996* (European Physical Society, Geneva, 1996).
[8] C. O. Weiss, ESPRIT LTR Project PASS report.
[9] J. L. Oudar, B. Sfez, R. Kuszelewicz, J. C. Michael, and R. Azoulay, Appl. Phys. Lett. **57**, 324 (1990).
[10] V. Pellegrini, F. Fuso, E. Arimondo, F. Castelli, L. A. Lugiato, G. P. Bava, and P. L. Debernardi, Phys. Rev. A **50**, 5219 (1994).
[11] F. Prati, A. Tesei, L. A. Lugiato, and R. J. Horowicz, Chaos Solitons Fractals **4**, 1637 (1994), and references therein.